Biointerface Research in Applied Chemistry
Platinum Open Access Journal (ISSN: 2069-5837)

Article
Volume 12, Issue 5, 2022, 5953 - 5968
https://doi.org/10.33263/BRIAC125.59535968

DFT Studies and Molecular Dynamics of the Molecular and Electronic Structure of Cu (II) and Zn (II) Complexes with the Symmetric Ligand (Z)-2-((3,5-dimethyl-2H-pyrrol-2-yl) methylene)-3,5-dimethyl-2H-pyrrole.

Manos Vlasiou [1,*], Kyriaki S. Pafiti [1]

[1] Department of Life and Health Sciences, University of Nicosia, Nicosia 2417, Cyprus

* Correspondence: vlasiou.m@unic.ac.cy (M.V.);

Scopus Author ID 56019849700

Received: 10.08.2021; Revised: 10.10.2021; Accepted: 14.10.2021; Published: 2.11.2021

Abstract: The binding patterns of the metal cations Cu^{2+} and Zn^{2+} with the symmetric ligands (Z)-2-((3,5-dimethyl-2H-pyrrol-2-yl) methylene)-3,5-dimethyl-2H-pyrrole (L_1) and (Z)-2-(1-(3,5-dimethyl-2H-pyrrol-2-yl)ethylidene)-3,5-dimethyl-2H-pyrrole (L_2), have been investigated at B3LYP and MM2 level of theories in the gas phase and a solution respectively. Natural bond orbital (NBO) analysis has been applied to explore the character of metal-ligand coordination. The stability of the most favorable binding motifs of the metal ions has also been investigated by the molecular dynamics (MD) simulation. Finally, the inhibition activity of the complexes (L_1Cu^{2+}), (L_2Cu^{2+}), (L_1Zn^{2+}), and (L_2Zn^{2+}) against the DNA dependent protein kinase also have been investigated by molecular docking studies.

Keywords: DFT; MD; pyrrole; zinc; copper; computational chemistry.
Abbreviations: DFT: Density Functional Theory; MD: Molecular Dynamics; NBO: Natural Bond Orbital; RMSD: Root-Mean Square deviation.

1. Introduction

N-heterocycles are the foremost common structural skeletons of licensed drugs on the market. 84% of the full number of molecules contain a minimum of one nitrogen atom, while 59% contain at least one nitrogen heterocycle [1]. Heterocyclic compounds can be inorganic, organic, containing one carbon atom and one or more atoms of elements aside from carbon, such as sulfur, oxygen, and nitrogen within the ring structure [2]. Pyrrole-type structures can be used or modified chemically to accommodate the particular steric and electronic demands at the metal atom (as a ligand). Secondly, the resulting metal complexes can exhibit enhanced thermal and chemical stability, rendering them ideal for small molecule activation and catalysis [3].

Cu^{2+} and Zn^{2+} metal ions have similar ionic radii [4] and participate in biological systems in a number of biochemical reactions. They also have the most role in cellular functions, cytochrome c oxidase, and a spread of pro-oxidant and antioxidant chemical reactions [4]. Two examples of zinc-containing enzymes are carbonic anhydrase and carboxypeptidase, which process the carbon dioxide (CO_2) regulation and digestion of proteins, respectively [5]. Carbonic anhydrase in vertebrates converts CO_2 into bicarbonate, and the same enzyme transforms the bicarbonate back into CO_2 for exhalation. Copper proteins have

multiple roles in biological electron transport and oxygen transportation, processes that exploit the easy interconversion of Cu (I) and Cu (II). In cytochrome c oxidase, copper and iron work together in aerobic respiration to reduce oxygen [6]. Copper is also found in Cu/Zn superoxide dismutase, an enzyme that detoxifies superoxides by transforming them to oxygen and hydrogen peroxide. Copper is also a component of lysyl oxidase, an enzyme that synthesizes collagen and elastin, two important structural proteins found in bone and connective tissue [7].

Conversely, pyrroles are vigorous components of complex macrocycles, including the porphyrins of heme, chlorins, bacteriochlorins, chlorophyll, porphyrinogens, making them a privileged scaffold with assorted nature of biological activities [8]. Pyrrole and its derivatives are known for inhibiting the reverse transcriptase (human immunodeficiency virus type 1 (HIV-1)) and cellular DNA-dependent protein kinases, exhibiting a wide range of biological activities such as antibacterial, anti-fungal, anti-viral, anti-inflammatory, anticancer, and antioxidant activity [9]. Based on these findings, this study aims to study theoretically (using density functional theory and molecular dynamics) the molecular characterization of unique metal-based complexes obtained by the reaction of the symmetric ligands (Z)-2-((3,5-dimethyl-2H-pyrrol-2-yl) methylene)-3,5-dimethyl-2H-pyrrole and (Z)-2-(1-(3,5-dimethyl-2H-pyrrol-2-yl)ethylidene)-3,5-dimethyl-2H-pyrrole with the copper (II) and zinc (II) metal ions. Additional work on the biological role of these systems is provided, using molecular docking studies, comparing the inhibition of cellular DNA-dependent protein kinase before and after complexation of the pyrrole derivatives with Cu^{2+} and Zn^{2+}metal ions.

2. Materials and Methods

The structures of (Z)-2-((3,5-dimethyl-2H-pyrrol-2-yl) methylene)-3,5-dimethyl-2H-pyrrole (**L_1**) and (Z)-2-(1-(3,5-dimethyl-2H-pyrrol-2-yl)ethylidene)-3,5-dimethyl-2H-pyrrole (**L_2**) (Cu^{2+}/Zn^{2+}) complexes were optimized at B3LYP/6-31++G(d,p) level of theory [10, 11] using ORCA [12] program. To count the deviation of the electronic spatial extent or dispersion energy, we have also calculated the structural energy at the MM2 level of theories, and the results were compared with the structural energy obtained at B3LYP/6-31+g(d) [13] for the binding of Cu^{2+}, and Zn^{2+} with **L_1** and **L_2**. Natural bond orbital (NBO) analysis [14] has also been done for the evaluation of the orbital contribution of the possible donor atoms of ligands to the metal cations for different conformers of the complexes. Additionally, dynamic molecular studies were performed using Abalone software, at 1 atm atmosphere, the temperature of 298 K, 1.00 MD step (fs), 1000 MD steps per trial, and duration of 100000 ps, to get a further inside of the stability of the structures.

Finally, molecular docking was performed using iGEMDOCK [15, 16], discovering the binding inhibition activity of the metal complexes with 7K11 (CryoEM structure of inactivated-form FATKIN domain of DNA-PK) from the protein data bank. In view to verify the interactions and stability between the kinase and its potential inhibitors, the kinase inhibitors used here, explicit solvent molecular dynamics simulations were carried out with Abalone package.

3. Results and Discussion

The cations of Cu^{II} and Zn^{II} are strongly involved in cation-π interaction and are also able to force both the C=N group into chelation by overcoming any steric strain and entropic drawback to achieving structures with increased stability [17]. Both of these pyrrole ligands

have bidentate binding motifs. For the chelation of highly charged metal cations with the pyrrole derivatives (acting as ligands), we should consider the sharing binding pattern of metal cations to the nitrogen atom of the pyrrole ring. We were mainly interested in determining the most favorable binding sites for the interaction of Cu^{II} and Zn^{II} with the pyrrole derivatives **L_1** and **L_2** (Figure 1). We have optimized the coordination patterns of the metal ions without putting any constrain. The relative energy of all promising structures is presented in Table 1. The relative energy was calculated considering zero points that corrected structural energy.

Table 1. Energies of the complex structures, calculated by MM2 level of theories.

$[(L_1)_2Cu^{II}]$ (Kcal/mol)	**$[(L_2)_2Cu^{II}]$ (Kcal/mol)**	**$[(L_1)_2Zn^{II}]$ (Kcal/mol)**	**$[(L_2)_2Zn^{II}]$ (Kcal/mol)**
Stretch: 101.2314	Stretch: 11.3448	Stretch: 326.4988	Stretch: 324.6708
Bend: 150.7152	Bend: 290.4168	Bend: 150.0973	Bend: 154.4804
Stretch-Bend: -0.3425	Stretch-Bend: -0.0750	Stretch-Bend: -1.4231	Stretch-Bend: -3.1855
Torsion: 208.5342	Torsion: 214.1282	Torsion: 166.1569	Torsion: 170.4706
Non-1,4 VDW: 6.8120	Non-1,4 VDW: 23.4715	Non-1,4 VDW: 494.2929	Non-1,4 VDW: 446.5972
1,4 VDW: 120.1208	1,4 VDW: 139.9779	1,4 VDW: 122.5540	1,4 VDW: 169.5246
Dipole/Dipole: 2.9805	Dipole/Dipole: 3.8702	Dipole/Dipole: 0.8702	Dipole/Dipole: 0.9805
Total Energy: 590.0515	Total Energy: 683.1343	Total Energy: 1258.1769	Total Energy: 1262.5581

The relative energy profile for all binding patterns of the ligands with the metal ions is found between (590.00 -17664.00 Kcal/mol) energy limits. The $[L_1Cu^{II}]$ system was found as the most favorable structure at B3LYP, while the $[L_1Zn^{II}]$ was found as the most favorable conformer at the MM2 level of theory. More specifically, for the B3LYP model of theory, the order of the stability of the systems was $[L_2Zn^{II}]$> $[L_2Cu^{II}]$> $[L_1Cu^{II}]$> $[L_1Zn^{II}]$. Regarding the MM2 level of theory, the order of stability of the systems was $[L_1Cu^{II}]$> $[L_2Cu^{II}]$> $[L_1Zn^{II}]$> $[L_2Zn^{II}]$. We can see some differences here in the calculated values since B3LYP calculates the structures of the molecules in the gas phase while MM2 (molecular mechanics modeling) calculates the structure in a solution. In the gas phase, the extra $-CH_3$ group of L_2 does not interfere with the system's stability.

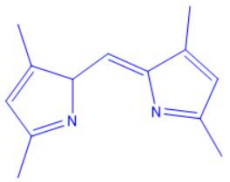

(*Z*)-2-((3,5-dimethyl-2*H*-pyrrol-2-yl)methylene)-3,5-dimethyl-2*H*-pyrrole

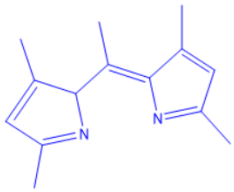

(*Z*)-2-(1-(3,5-dimethyl-2*H*-pyrrol-2-yl)ethylidene)-3,5-dimethyl-2*H*-pyrrole

Figure 1. Structures of the studied ligand molecules **L_1** and **L_2**.

Here the system responds differently on the metal electron acceptor zinc and copper. The methyl group distorts the system much more in a solution, playing an important role in the

stability energies. The two ligands used are depicted in Figure 1**.** The values of relative energy calculated at the MM2 level of theory are different from those obtained using the B3LYP level of theory. The same thing is observed for both metal ions. Despite this, the order of stability of the four metal complexes is the same for both methods. Therefore, the deviation of electronic dispersion energy is not high enough to change the stability order of the metal complexes.

To identify the active minimum at the potential energy surface of each complex molecule, we have monitored the average value of coordination length for a certain time interval, where the coordination length showed high consistency in the bonding. Molecular dynamics simulations revealed that $[(L_1)_2Cu^{II}]$ complex molecule has a total Energy equal to -11569.8 kcal/mol. Regarding $[(L_2)_2Cu^{II}]$ complex molecule, the energy was equal to -11575.9 kcal/mol, which is very close to $[(L_1)_2Cu^{II}]$. Regarding the Zn^{II} complexes, for $[(L_1)_2Zn^{II}]$, the energy was equal to -11239.1 kcal/mol, while for the $[(L_2)_2Zn^{II}]$ molecule, total energy was equal to -17664.1 kcal/mol. Here, the water implication in the method revealed that $[(L_2)_2Zn^{II}]$ is the most stable structure compared to the other three. The extra methyl group on the pyrrole derivative L_2 seems to stabilize the structure better. The local active energy minimum and the coordination length of the metal cations in pyrrole complexes were found to be the same as obtained from the DFT calculations.

Before the complexation of the ligands with the metal ions, a calculation has been performed to identify the IR (Figure 2) spectrums completing their structural profile. As we can see from the IR spectrums, the L_1, (Z)-2-((3,5-dimethyl-2H-pyrrol-2-yl) methylene)-3,5-dimethyl-2H-pyrrole gave a strong peak at 1737 nm, which belongs to the C=O stretching group, while the peak at 2000 nm corresponds to the C=N stretching group [18]. Medium peaks from 2800-3000 nm are because of the C-H stretching groups of the pyrrole derivative. Regarding the IR spectrum of L_2, (Z)-2-(1-(3,5-dimethyl-2H-pyrrol-2-yl)ethylidene)-3,5-dimethyl-2H-pyrrole, we can see two extra peaks at 2200 and 2400 nm probably because of the distortion of the system because of the extra methyl group on the pyrrole moiety [19].

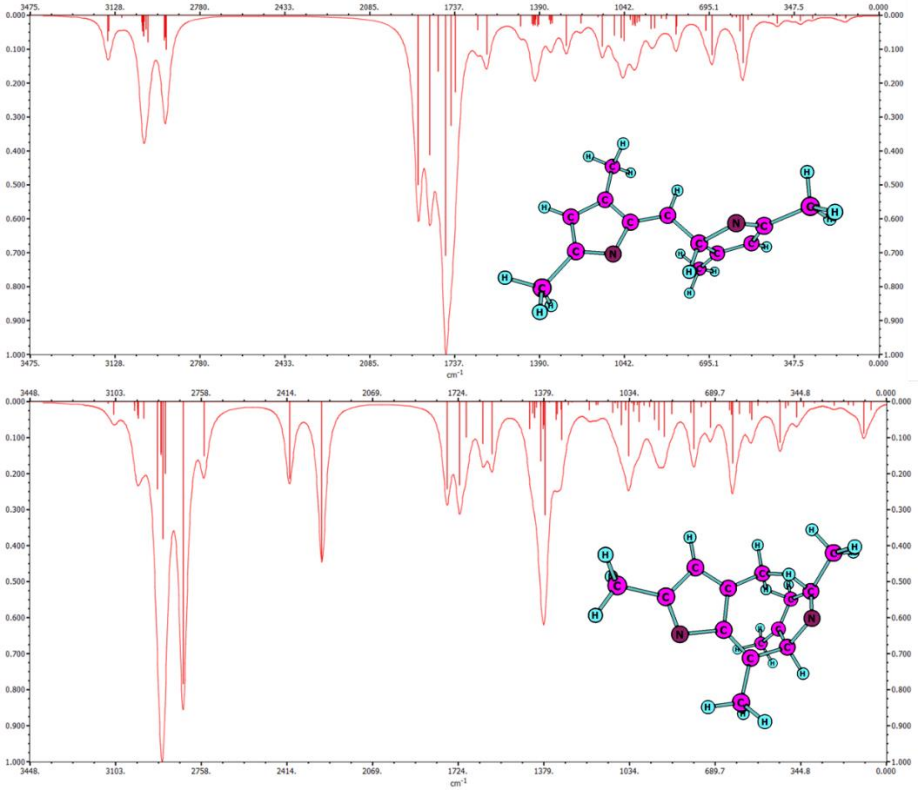

Figure 2. Calculated IR spectrums of the ligands **L_1** and **L_2**.

Regarding the calculated NMR chemical shifts of the ligands and the spectrums, can be found in supplementary in Figure S1. The geometrical parameters such as bond lengths and bond angles of the complexed molecules derived from DFT calculations can be found also in Table S1, S2, S3, and S4. Here in Table 2, we can see some selected bond lengths of the four complexes. Some changes in the bond lengths of the metals with the chorine and the nitrogen are observed because of the change in entropy of the system as the second ligand coordinates to the metal ions. The actual 3d structures with numbered atoms can be seen in Figure 3 regarding the copper (II) complexes and Figure 4 regarding the zinc (II) complexes.

Table 2. Selected bond lengths of the studied molecules at MM2 level of theory.

$[(L_1)_2Cu^{II}]$		**$[(L_2)_2Cu^{II}]$**		**$[(L_1)_2Zn^{II}]$**		**$[(L_2)_2Zn^{II}]$**	
Bond Length (Å)		*Bond Length (Å)*		*Bond Length (Å)*		*Bond Length (Å)*	
Cu(35)-Cl(37)	2.2163	Cu(35)-Cl(37)	2.192	Zn(35)-Cl(37)	2.269	Zn(35)-Cl(37)	2.2803
Cu(35)-Cl(36)	2.2355	Cu(35)-Cl(36)	2.2093	Zn(35)-Cl(36)	2.2649	Zn(35)-Cl(36)	2.2342
Cu(35)-N(26)	1.5415	Cu(35)-N(26)	1.4994	Zn(35)-N(26)	1.9879	Zn(35)-N(26)	1.9974
N(9)-Cu(35)	1.5344	N(9)-Cu(35)	1.5554	N(9)-Zn(35)	1.9521	N(9)-Zn(35)	1.9295
Cu(35)-N(21)	1.5017	Cu(35)-N(21)	1.4868	Zn(35)-N(21)	1.9254	Zn(35)-N(21)	1.9348
N(4)-Cu(35)	1.4773	N(4)-Cu(35)	1.4893	N(4)-Zn(35)	1.9302	N(4)-Zn(35)	1.9478

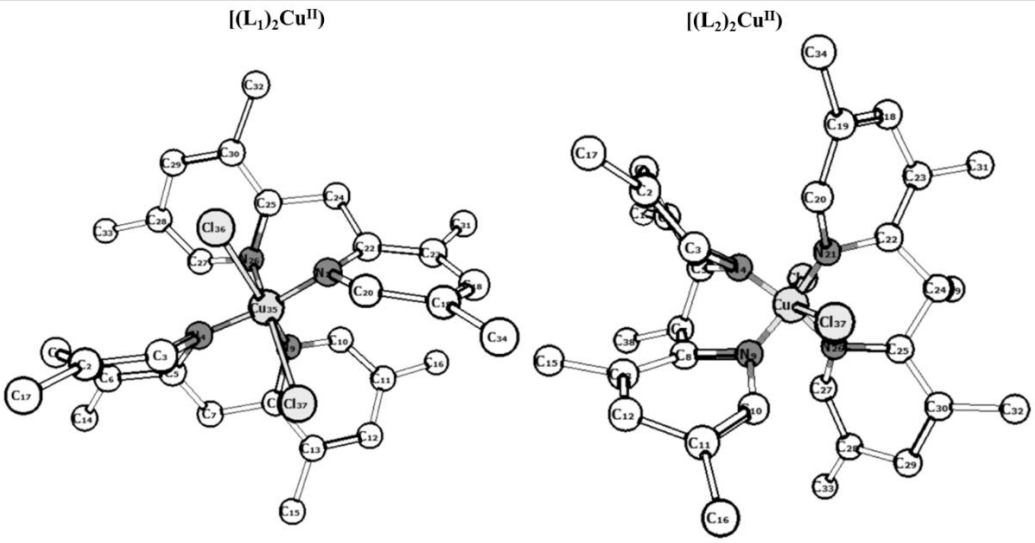

Figure 3. Complex molecules after the interaction of the **L_1** and **L_2** with Cu^{II}.

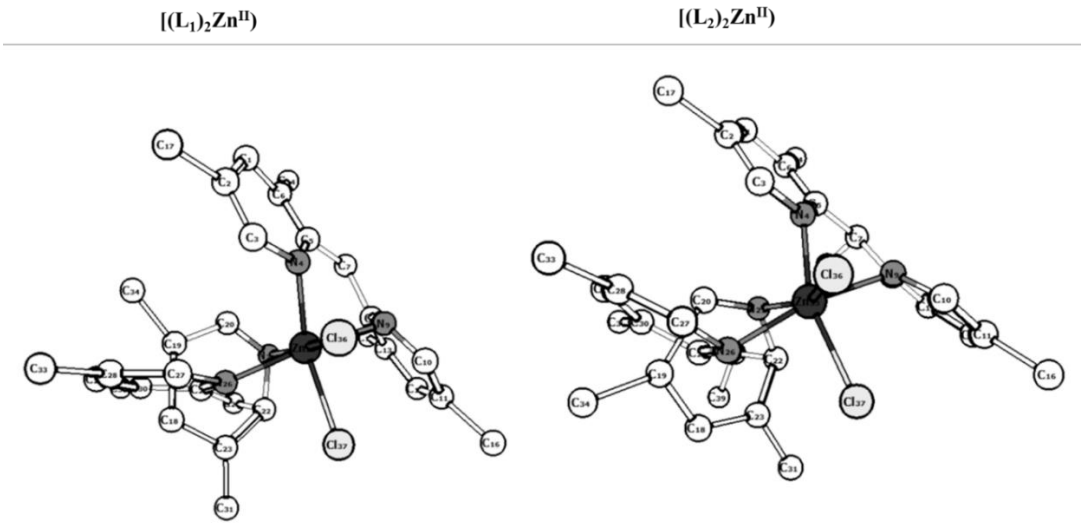

Figure 4. Complex molecules after the interaction of the **L_1** and **L_2** with Zn^{II}.

The Cu ^{II} complexes of the pyrrole derivatives [$(L_1)_2Cu^{II}$) and [$(L_2)_2Cu^{II}$) coordinated at a tetrahedral geometry while the complexes Zn^{II} complexes [$(L_1)_2Zn^{II}$) and [$(L_2)_2Zn^{II}$)] have a trigonal planar geometry as we can see in Figure 3 and 4 respectively.

Regarding the calculations at the B3LYP level of theory, we can observe the energies of the complexes in Table 3.

Table 3. Energies of the complex structures, calculated by the B3LYP level of theories.

TOTAL SCF ENERGY	**$[(L_1)_2Cu^{II}]$**	**$[(L_2)_2Cu^{II}]$**	**$[(L_1)_2Zn^{II}]$**	**$[(L_2)_2Zn^{II}]$**
Total Energy (eV)	-102753.80544	-105226.62078	-106821.39979	-108615.94854
Nuclear Repulsion (eV)	152344.96899	166245.11343	146341.38902	159962.25137
Electronic Energy (eV)	-255098.77443	-271471.73421	-253162.78881	-268578.19991
One Electron Energy (eV)	-444652.15190	-475432.03386	-435492.49343	-465209.73576
Two Electron Energy (eV)	-189553.37747	203960.29964	182329.70462	196631.53586
Potential Energy (eV)	-205553.88152	-210399.48413	-213494.84506	-217183.57257
Kinetic Energy (eV)	102800.07607	105172.86335	106673.44527	108567.62404

Atomic charges calculated for the study's structures are employed for describing the charge transfer and the electronegativity term [20]. The evaluation of the atomic charges is crucial for applying quantum chemical calculations to molecular systems. In the present work, we have calculated the atomic charges in two methods. So, we got the Mulliken and Loewdin atomic charges. Even though the charges due to the method's different developmental ways were not agreed to, the highest positive and highest negative values were for the same atoms, indicating the N atom as a donor to the metal ions. The atomic charge values for the four complex molecules can be found in the supplementary tables, Table S5 and Table S6.

In Table 2 and Table 4, we can see selected bond lengths of the coordination sphere of the structures calculated by MM2 and B3LYP level theories, respectively. Keeping in mind that in the gas phase, no solvent affects the system's entropy, we can explain the differences in bond lengths in both calculations. At the MM2 level of theory, most bond lengths are greater than 1 Å. On the other hand, in the gas phase, the bond lengths are smaller than 1 Å.

Table 4. Selected bond lengths of the studied molecules at the B3LYP level of theory.

$[(L_1)_2Cu^{II}]$		**$[(L_2)_2Cu^{II}]$**		**$[(L_1)_2Zn^{II}]$**		**$[(L_2)_2Zn^{II}]$**	
Bond Length (Å)		*Bond Length (Å)*		*Bond Length (Å)*		*Bond Length (Å)*	
Cu(35)-Cl(37)	0.6754	Cu(35)-Cl(37)	0.8917	Zn(35)-Cl(37)	0.8003	Zn(35)-Cl(37)	0.4257
Cu(35)-Cl(36)	0.4522	Cu(35)-Cl(36)	1.0916	Zn(35)-Cl(36)	0.7820	Zn(35)-Cl(36)	0.4851
Cu(35)-N(26)	0.4636	Cu(35)-N(26)	0.2468	Zn(35)-N(26)	0.5801	Zn(35)-N(26)	0.3642
N(9)-Cu(35)	0.5072	N(9)-Cu(35)	0.1506	N(9)-Zn(35)	0.5865	N(9)-Zn(35)	0.1942
Cu(35)-N(21)	0.4383	Cu(35)-N(21)	1.0916	Zn(35)-N(21)	0.4301	Zn(35)-N(21)	0.2523
N(4)-Cu(35)	0.3112	N(4)-Cu(35)	0.4530	N(4)-Zn(35)	0.4208	N(4)-Zn(35)	0.1265

HOMO refers to the outermost orbital filled with electrons, and it is connected to the ionization potential, acting as an electron donor. The LUMO is the first empty innermost orbital unfilled by an electron, and it is directly connected with the electron affinity, acting as an electron acceptor [21]. The energy gap between the HOMO and LUMO's energies specifies the molecular chemical stability representing a very important parameter employed to determine the molecular electrical transport properties. Thus, compounds showing a large energy gap between HOMO and LUMO are known as "hard molecules", while chemical entities having small HOMO-LUMO energy gaps are considered "soft molecules". Accordingly, a compound with the smallest energy difference between HOMO and LUMO is considered more reactive [22]. Here, we have calculated the HOMO-LUMO energies in two ways, with the Huckel

calculation and DFT studies at the B3LYP level of theory. In Figure 5, the HOMO-LUMO orbitals of the Zn ^{II} complexes are depicted, while in Figure 6, we see the HOMO-LUMO orbitals of the Cu ^{II} complexes. Additionally, in Table 5, we can see the electronic descriptors of the studied complex molecules calculated in both ways.

Table 5. Electronic descriptors for the studied complex molecules.

Molecules at MM2	HOMO (eV)	LUMO (eV)	Δgap (eV)
$[(L_1)_2Cu^{II}]$	-2.493	-0.105	-2.388
$[(L_2)_2Cu^{II}]$	-2.043	-0.103	-1.940
$[(L_1)_2Zn^{II}]$	0.130	0.673	-0.543
$[(L_2)_2Zn^{II}]$	0.155	0.486	-0.331
Molecules at B3LYP	**HOMO (eV)**	**LUMO (eV)**	**Δgap (eV)**
$[(L_1)_2Cu^{II}]$	26.8827	27.2687	-0.3860
$[(L_2)_2Cu^{II}]$	53.3747	53.5006	-0.1259
$[(L_1)_2Zn^{II}]$	47.2774	47.3977	-0.1203
$[(L_2)_2Zn^{II}]$	17.4684	17.5812	-0.1128

Based on our findings, $[(L_1)_2Cu^{II}]$ seems to be the most reactive of the four substances, followed by $[(L_2)_2Cu^{II}]$, $[(L_1)_2Zn^{II}]$, and $[(L_2)_2Zn^{II}]$. The same trend is followed in both calculation ways, although the numbers are different due to the way the values are calculated. It is worthy of mentioning here that the extra methyl group of L_2 makes the molecules "hard", but in general, the Zn ions seem to stabilize the structures more.

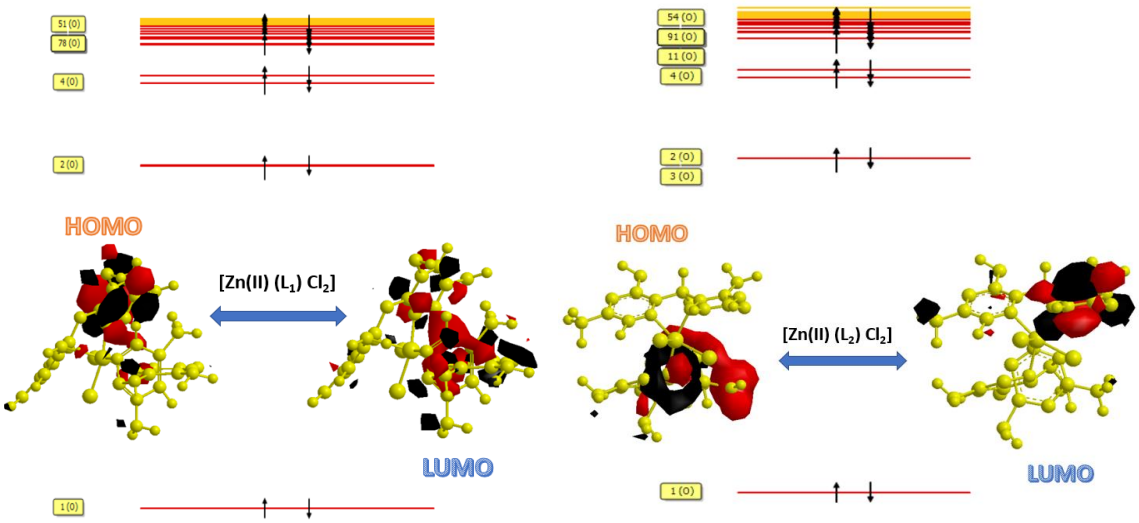

Figure 5. HOMO-LUMO orbitals of the Zn II complexes.

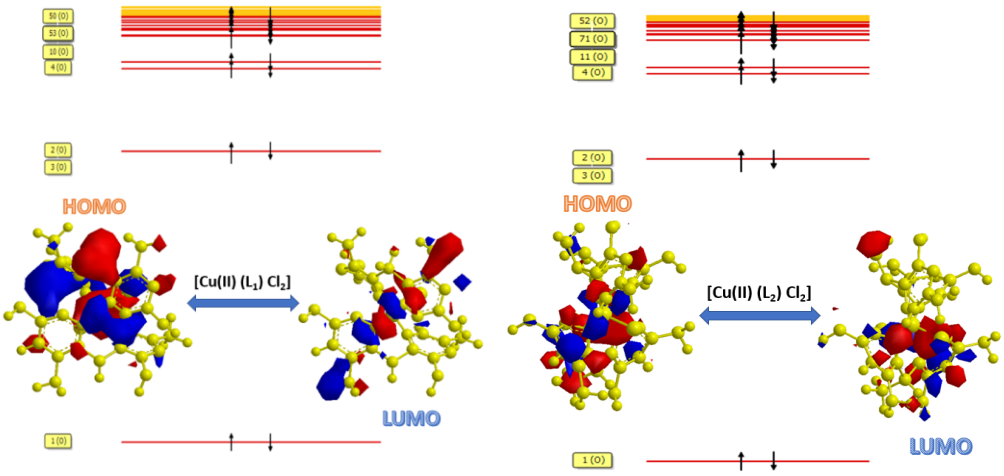

Figure 6. HOMO-LUMO orbitals of the Cu ^{II} complexes.

Molecular docking and dynamics are the core part of designing and screening new bioactive molecules [23]. We decided to screen the binding affinity of the four studied complex molecules with the DNA-dependent protein kinase (DNA-PK). As a member of the phosphatidylinositol 3-kinase-related kinase (PIKK) family, DNA-PK is best referred to as a medium of the cellular response to DNA damage [24, 25]. Beyond the DNA damage response, DNA-PK activity is necessary for various cellular functions, including the regulation of transcription, progression of the cell cycle, and the maintenance of telomeres. Thus, to explore the possible biological significance of these molecules, we have performed docking studies followed by molecular dynamics to know the internal motions, conformational changes, and stability of protein-ligand complexes. Figure 7 depicts the domain of the DNA-PK, that we used for our studies. In Table 6, we can see the calculated results of the docking studies.

Interestingly we can observe that the total energy of the complexation lies only on hydrophobic interactions. Some electrostatic interactions are incorporated for L_1 and L_2 only. Regarding the studied molecules, the complexation of L_1 with the metal ions does not seem to improve the binding affinity of the molecules with the protein. On the other hand, regarding L_2, it seems that the complexation with metal ions increases the binding affinity, mostly after the complexation with Cu^{II} metal ions. Even though metal complexation increases the hydrophobicity of the molecules and the main energy contribution here are the van der Waals interactions, this does not seem to improve the binding affinity of L_1, which means that the extra methyl group of the L_2 stabilizes better the structures and contributes to the binding affinity.

Table 6. Binding affinities energies of the DNA-PK with the studied molecules.

Protein-Ligand Complex	Total Energy (Kcal/mole)	VDW (Kcal/mole)	Electrostatics (Kcal/mole)
7k11-L_1	-82.1716	-74.3473	-7.82432
7k11-[$(L_1)_2Cu^{II}$]	-80.4914	-80.4914	
7k11-[$(L_1)_2Zn^{II}$]	-76.9008	-76.9008	
7k11-L_2	-69.7404	-62.7724	-6.968
7k11-[$(L_2)_2Cu^{II}$]	-74.8688	-74.8688	
7k11-[$(L_2)_2Zn^{II}$]	-72.395	-72.395	

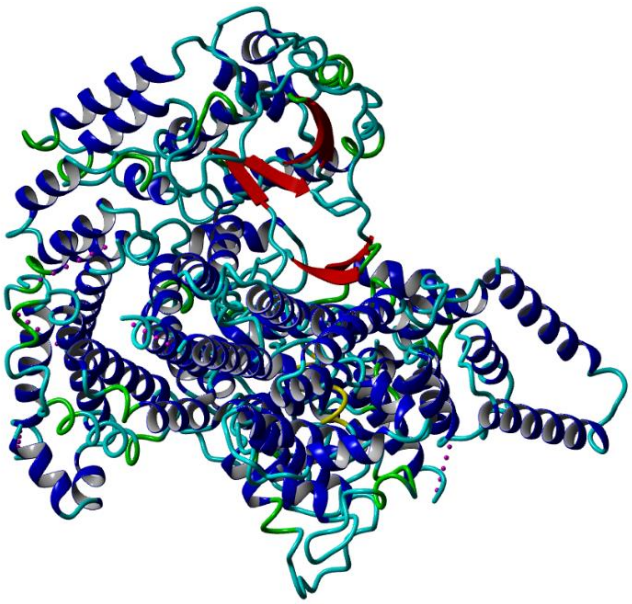

Figure 7. Structure of the DNA-PK domain protein (PDB:7K11).

The RMSD values give insides of the fluctuations during the binding process [26]. Small fluctuations indicate a stable conformation. Actually, [$(L_1)_2Cu^{II}$] gave an average RMSD

value of 0.432 Å, $[(L_1)_2Zn^{II}]$ 0.239 Å, $[(L_2)_2Cu^{II}]$ 0.278 Å and $[(L_2)_2Zn^{II}]$ 0.495 Å. These results show stable conformation by all the complexes. The overall stability of these complexes increases with a decrease in their mean values of RMSD as follows: $[(L_1)_2Zn^{II}] > [(L_2)_2Cu^{II}] > [(L_1)_2Cu_{II}] > [(L_2)_2Zn_{II}]$ with the studied protein.

4. Conclusions

In this work, we have calculated the energies of four new complexes, baring pyrrole derivatives as chelators and Cu ^{II} and Zn ^{II} metal ions, to form stable structures. The energies have been investigated by the MM2 and B3LYP levels of theories. Additionally, we have performed molecular dynamics simulations that were found to agree with the DFT studies regarding the total energies. More specifically, for the B3LYP model of theory, the order of the stability of the systems was $[L_2Zn^{II}]> [L_2Cu^{II}]> [L_1Cu^{II}]> [L_1Zn^{II}]$. Regarding the MM2 level of theory, the order of stability of the systems was $[L_1Cu^{II}]> [L_2Cu^{II}]> [L_1Zn^{II}]> [L_2Zn^{II}]$. After performing NBO analysis, we found that $[L_1Cu^{II}]$ seems to be the most reactive of the four substances, followed by $[L_2Cu^{II}]$, $[L_1Zn^{II}]$, and $[L_2Zn^{II}]$. Finally, the docking results showed hydrophobic interactions between the complex molecules and the DNA-PK, increasing the binding affinity after complexation with metal ions for the L_2 molecule.

Funding

None.

Acknowledgments

None.

Conflicts of Interest

The authors have no conflicts of interest to declare that they are relevant to the content of this article.

References

1. Li Petri, G.; Spanò, V.; Spatola, R.; Holl, R.; Raimondi, M.V.; Barraja, P.; Montalbano, A. Bioactive pyrrole-based compounds with target selectivity. *Eur J Med Chem*. **2020,** *208*, 112783, https://doi.org/10.1016/j.ejmech.2020.112783.
2. Bhardwaj, V.; D. Gumber.; V. Abbot.; S. Dhiman.; P. Sharma. Pyrrole: A resourceful small molecule in key medicinal hetero-aromatics. *RSC Adv.* **2015**, *5*, 15233–15266, https://doi.org/10.1039/c4ra15710a.
3. Ehrlich, N.; Freytag, M.; Raeder, J.; Jones, P.G.; Walter, M.D. Pyrrole-based pincer ligands containing iminophosphorane moieties and their coordination chemistry with group 1 metals and magnesium. *Zeitschrift Fur Anorg. Und Allg. Chemie*. **2021**, *647*, 1462–1470, https://doi.org/10.1002/zaac.202100080.
4. Mayhugh, J.T.; Niklas, J.E.; Forbes, M.G.; Gorden, J.D.; A.E.V. Gorden. Pyrrophens: Pyrrole-Based Hexadentate Ligands Tailor-Made for Uranyl (UO22+) Coordination and Molecular Recognition. *Inorg. Chem.* **2020**, *59*, 9560–9568. https://doi.org/10.1021/acs.inorgchem.0c00439.
5. Kaur, R.; Rani, V.; Abbot, V.; Kapoor, Y.; Konar, D.; K. Kumar. Recent synthetic and medicinal perspectives of pyrroles: An overview. *J. Pharm. Chem. Chem. Sci* **2017**, *1*, 17–32, https://www.alliedacademies.org/articles/recent-synthetic-and-medicinal-perspectives-of-pyrroles-an-overview-9135.html.
6. Imafuku, M.; Oki, S.; Suzuki, M. Bromine-Terminated β-Alkyl-Substituted Tripyrrin: Reactivity, Coordination Ability, and Role as Extendable Acyclic Oligo-Pyrrole Ligand. *ChemistrySelect.* **2020**, *5*, 7217–7221, https://doi.org/10.1002/slct.202001412.

7. Osredkar, J.; Sustar, N. Copper and Zinc, Biological Role and Significance of Copper/Zinc Imbalance. *J. Clin. Toxicol.* **2011**, *s3*, 1–18, https://doi.org/10.4172/2161-0495.s3-001.
8. Wei, J.; Cao, B.; Tse, C.W.; Chang, X.Y.; Zhou, C.Y.; Che, C.M. Chiral: Cis -iron(ii) complexes with metal-And ligand-centered chirality for highly regio- And enantioselective alkylation of N-heteroaromatics. *Chem. Sci.* **2020**, *11*, 684–693, https://doi.org/10.1039/c9sc04858h.
9. Maaß,C.; Andrada, D.M.; Mata, R.A.; Herbst-Irmer, R..; Stalke, D. Effects of metal coordination on the π-system of the 2,5-bis-{(pyrrolidino)-methyl}-pyrrole pincer ligand. *Inorg. Chem.* **2013**, *52*, 9539–9548, https://doi.org/10.1021/ic401192x.
10. Camacho-Mendoza, R.L.; Aquino-Torres, E.; Cruz-Borbolla, J.; Alvarado-Rodríguez, J.G.; Olvera-Neria, O.; Narayanan, J.; Pandiyan, T. DFT analysis: Fe4 cluster and Fe(110) surface interaction studies with pyrrole, furan, thiophene, and selenophene molecules. *Struct. Chem*. **2014**, *25*, 115–126, https://doi.org/10.1007/s11224-013-0254-9.
11. Guo, J.; Deng, X.; Song. C.; Lu, Y.; Qu, S.; Dang, Y.; Wang, Z.X. Differences between the elimination of early and late transition metals: DFT mechanistic insights into the titanium-catalyzed synthesis of pyrroles from alkynes and diazenes. *Chem. Sci.* **2017**, *8*, 2413–2425, https://doi.org/10.1039/c6sc04456e.
12. Neese, F.; Wennmohs, F.; Becker, U.; Riplinger, C. The ORCA quantum chemistry program package. *J. Chem. Phys.* **2020**, *152*, 1–18, https://doi.org/10.1063/5.0004608.
13. Tziouris, P.A.; Tsiafoulis, C.G.; Vlasiou, M.; Miras, H.N.; Sigalas, M.P.; Keramidas, A.D.; Kabanos, T.A. Interaction of Chromium(III) with a N, N ′-disubstituted hydroxylamine-(diamido) ligand: A combined experimental and theoretical study. *Inorg. Chem.* **2014**, *53*, 11404–11414, https://doi.org/10.1021/ic501778d.
14. Mirzaeva, I. V.; Kozlova, S.G.; Krisyuk, V. V. Quantum Chemical Study of the Stability of Copper-Palladium Complexes in the Gas Phase. *J. Struct. Chem.* **2021**, *62*, 9–18, https://doi.org/10.1134/S0022476621010029.
15. Yang, J.M.; Chen, C.C. GEMDOCK: A Generic Evolutionary Method for Molecular Docking. *Proteins Struct. Funct. Genet.* **2004**, *55* 288–304, https://doi.org/10.1002/prot.20035.
16. Sulpizi, M.; Schelling, P.; Folkers, G.; Carloni, P.; Scapozza, L. The Rational of Catalytic Activity of Herpes Simplex Virus Thymidine Kinase. *J. Biol. Chem.* **2001**, *276*, 21692–21697, https://doi.org/10.1074/jbc.m010223200.
17. Bhunia, S.; Kumar, A.; Singh, A.; Ojha, A.K. Binding patterns of metal cations (Na+, K+, Cu2+, and Zn2+) with Trp-Trp di-peptide investigated by DFT, NBO, and MD simulation. *Comput. Theor. Chem.* **2018**, *1141*, 7–14, https://doi.org/10.1016/j.comptc.2018.08.010.
18. Samy, F.; Omar, F.M. Synthesis, characterization, antitumor activity, molecular modeling and docking of new ligand, (2,5-pyrrole)-bis(5,6-diphenyl-[1,2,4]-triazin-3-yl)hydrazone and its complexes. *J. Mol. Struct.* **2020**, *1222*, 128910, https://doi.org/10.1016/j.molstruc.2020.128910.
19. Alturiqi, A.S.; Alaghaz, A.N.M.A.; Ammar, R.A.;. Zayed, M.E. Synthesis, Spectral Characterization, and Thermal and Cytotoxicity Studies of Cr(III), Ru(III), Mn(II), Co(II), Ni(II), Cu(II), and Zn(II) Complexes of Schiff Base Derived from 5-Hydroxymethylfuran-2-carbaldehyde. *Journal of Chemistry*. **2018,** *2018*, 5816906, https://doi.org/10.1155/2018/5816906.
20. Sen Gupta, P.S.; Bhat, H.R.; Biswal, S.; Rana, M.K. Computer-aided discovery of bis-indole derivatives as multi-target drugs against cancer and bacterial infections: DFT, docking, virtual screening, and molecular dynamics studies. *J. Mol. Liq.* **2020**, *320*, 114375, https://doi.org/10.1016/j.molliq.2020.114375.
21. Vlasiou, M.C.; Pafti, K.S. Screening possible drug molecules for Covid-19. The example of vanadium (III/IV/V) complex molecules with computational chemistry and molecular docking. *Comput. Toxicol.*, **2021**, *18*, 100157, https://doi.org/10.1016/j.comtox.2021.100157.
22. Sakib, S.A.; Khan, M.F.; Arman, M.; Bin Kader, F.; Faruk, M.O.; Tanzil, S.M.; Debnath, T.; Haque, M.A.; Brogi, S. Computer-based approaches for determining the pharmacological profile of 5-(3-nitro-arylidene)-thiazolidine-2,4-dione. *Biointerface Res. Appl. Chem.* **2021**, *11*, 13806–13828, https://doi.org/10.33263/BRIAC116.1380613828.
23. Farcaş, A.A.; Bende, A. Theoretical modeling of the singlet-triplet spin transition in different Ni(ii)-diketo-pyrphyrin-based metal-ligand octahedral complexes. *Phys. Chem. Chem. Phys.* **2021,** *23***,** 4784–4795, https://doi.org/10.1039/d0cp05366j.
24. Mohiuddin, I.S.; Kang, M.H.; DNA-PK as an Emerging Therapeutic Target in Cancer. *Front. Oncol.* **2019**, *9*, 1–8, https://doi.org/10.3389/fonc.2019.00635.
25. Chen, X.; Xu, X.; Chen, Y.; Cheung, J.C.; Wang, H.; Jiang, J.; de Val, N.; Fox, T.; Gellert, M.; Yang, W. Structure of an activated DNA-PK and its implications for NHEJ. *Mol. Cell*. **2021**, *81*, 801-810.e3, https://doi.org/10.1016/j.molcel.2020.12.015.
26. Bell, E.W.; Zhang, Y. DockRMSD: An open-source tool for atom mapping and RMSD calculation of symmetric molecules through graph isomorphism. *J. Cheminform*. **2019**, *11*, 1–9, https://doi.org/10.1186/s13321-019-0362-7.

Supporting Information

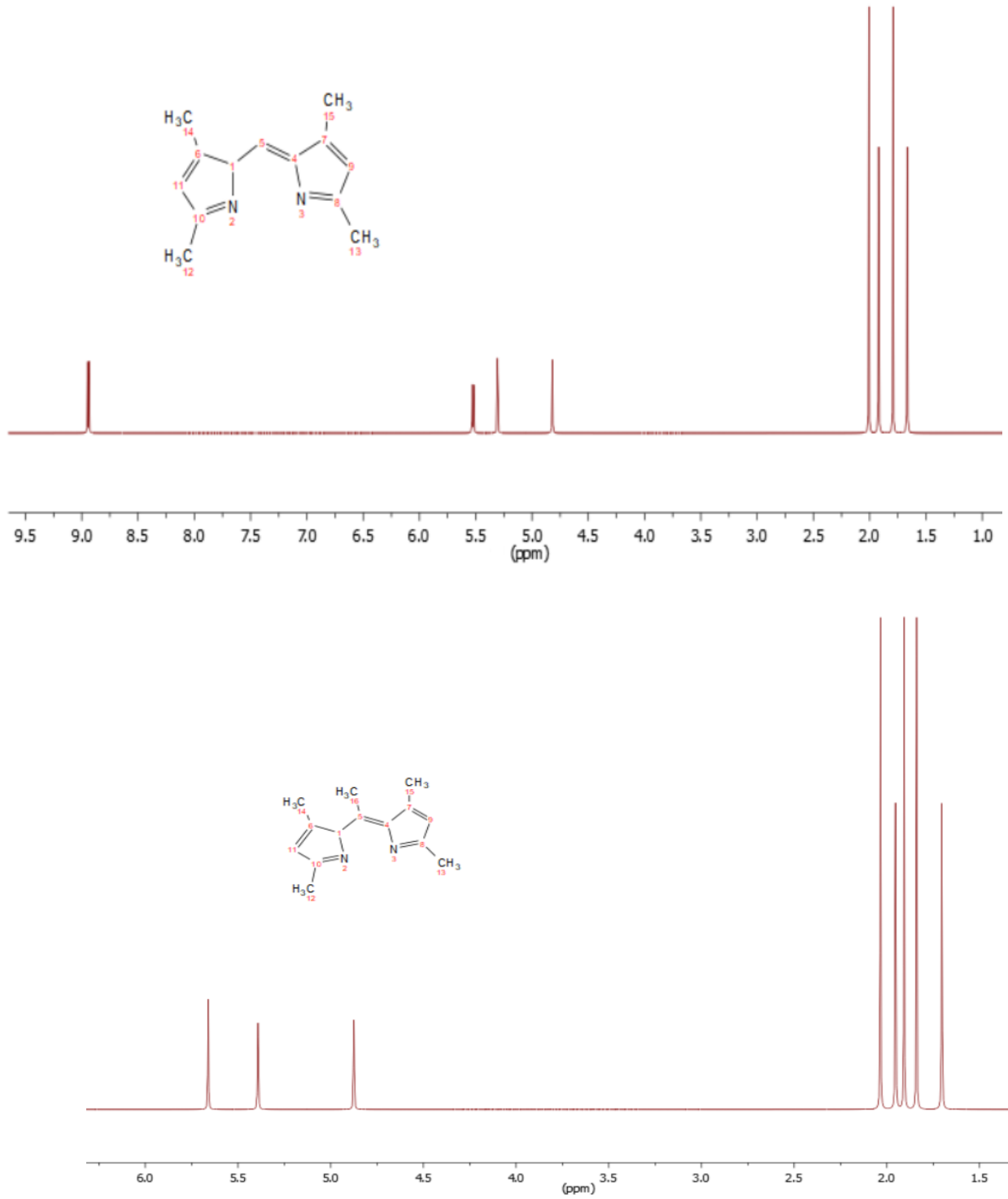

Figure S1. Calculated NMR spectrums for L_1 and L_2 pyrrole derivatives.

Table S1. Calculated bond lengths and bond angles for complex 1 [$(L_1)_2Cu^{II}$)].

Atoms	Bond Length (Å)	Atoms	Bond Angles (Å)	Atoms	Bond Angles (Å)
Cu(35)-Cl(37)	2.2163	Cl(37)-Cu(35)-Cl(36)	106.4388	C(12)-C(11)-C(10)	116.0802
Cu(35)-Cl(36)	2.2355	Cl(37)-Cu(35)-N(26)	168.9552	C(11)-C(10)-N(9)	130.2478
Cu(35)-N(26)	1.5415	Cl(37)-Cu(35)-N(9)	81.5528	Cu(35)-N(9)-C(10)	119.0316
N(9)-Cu(35)	1.5344	Cl(37)-Cu(35)-N(21)	86.9577	Cu(35)-N(9)-C(8)	122.2463
Cu(35)-N(21)	1.5017	Cl(37)-Cu(35)-N(4)	81.7074	C(10)-N(9)-C(8)	107.4144
N(4)-Cu(35)	1.4773	Cl(36)-Cu(35)-N(26)	84.5017	C(13)-C(8)-N(9)	127.7319
C(19)-C(34)	1.5102	Cl(36)-Cu(35)-N(9)	171.1554	C(13)-C(8)-C(7)	118.2506
C(28)-C(33)	1.5094	Cl(36)-Cu(35)-N(21)	77.2702	N(9)-C(8)-C(7)	113.7793

Atoms	Bond Length (Å)	Atoms	Bond Angles (Å)	Atoms	Bond Angles (Å)
C(30)-C(32)	1.5123	Cl(36)-Cu(35)-N(4)	76.6776	C(8)-C(7)-C(5)	109.0722
C(23)-C(31)	1.513	N(26)-Cu(35)-N(9)	87.4311	C(14)-C(6)-C(1)	114.2652
C(30)-C(25)	1.3536	N(26)-Cu(35)-N(21)	97.1591	C(14)-C(6)-C(5)	121.5997
C(29)-C(30)	1.3418	N(26)-Cu(35)-N(4)	99.773	C(1)-C(6)-C(5)	123.5019
C(28)-C(29)	1.3383	N(9)-Cu(35)-N(21)	107.4126	C(7)-C(5)-C(6)	116.5912
C(27)-C(28)	1.3448	N(9)-Cu(35)-N(4)	101.2076	C(7)-C(5)-N(4)	120.0919
N(26)-C(27)	1.2853	N(21)-Cu(35)-N(4)	147.2289	C(6)-C(5)-N(4)	122.3794
C(25)-N(26)	1.2865	C(32)-C(30)-C(25)	122.6594	Cu(35)-N(4)-C(5)	127.2957
C(24)-C(25)	1.5073	C(32)-C(30)-C(29)	119.3092	Cu(35)-N(4)-C(3)	128.7078
C(22)-C(24)	1.5057	C(25)-C(30)-C(29)	118.0178	C(5)-N(4)-C(3)	97.925
C(23)-C(18)	1.3393	C(30)-C(29)-C(28)	117.2284	N(4)-C(3)-C(2)	123.1263
C(22)-C(23)	1.3513	C(33)-C(28)-C(29)	120.5024	C(17)-C(2)-C(3)	119.5422
N(21)-C(22)	1.2817	C(33)-C(28)-C(27)	122.964	C(17)-C(2)-C(1)	117.4058
C(20)-N(21)	1.2883	C(29)-C(28)-C(27)	116.0899	C(3)-C(2)-C(1)	123.0272
C(19)-C(20)	1.3471	C(28)-C(27)-N(26)	128.9979	C(6)-C(1)-C(2)	96.6593
C(18)-C(19)	1.3379	Cu(35)-N(26)-C(27)	117.7572		
C(2)-C(17)	1.5124	Cu(35)-N(26)-C(25)	120.0207		
C(11)-C(16)	1.5111	C(27)-N(26)-C(25)	109.3142		
C(13)-C(15)	1.5144	C(30)-C(25)-N(26)	126.6945		
C(6)-C(14)	1.5162	C(30)-C(25)-C(24)	120.1803		
C(13)-C(8)	1.3556	N(26)-C(25)-C(24)	112.6359		
C(12)-C(13)	1.3392	C(25)-C(24)-C(22)	106.731		
C(11)-C(12)	1.3365	C(31)-C(23)-C(18)	119.3724		
C(10)-C(11)	1.347	C(31)-C(23)-C(22)	122.7958		
N(9)-C(10)	1.2853	C(18)-C(23)-C(22)	117.4565		
C(8)-N(9)	1.2872	C(24)-C(22)-C(23)	117.7327		
C(7)-C(8)	1.4925	C(24)-C(22)-N(21)	111.7185		
C(5)-C(7)	1.4924	C(23)-C(22)-N(21)	128.5869		
C(6)-C(1)	1.3618	Cu(35)-N(21)-C(22)	122.5253		
C(5)-C(6)	1.3653	Cu(35)-N(21)-C(20)	122.9541		
N(4)-C(5)	1.2901	C(22)-N(21)-C(20)	107.6295		
C(3)-N(4)	1.2983	N(21)-C(20)-C(19)	128.9723		
C(2)-C(3)	1.3588	C(34)-C(19)-C(20)	121.2454		
C(1)-C(2)	1.3625	C(34)-C(19)-C(18)	121.4729		
		C(20)-C(19)-C(18)	117.2472		
		C(23)-C(18)-C(19)	116.1229		
		C(15)-C(13)-C(8)	123.2006		
		C(15)-C(13)-C(12)	118.6046		
		C(8)-C(13)-C(12)	118.1812		
		C(13)-C(12)-C(11)	116.4804		
		C(16)-C(11)-C(12)	119.2557		
		C(16)-C(11)-C(10)	123.7902		

Table S2. Calculated bond lengths and bond angles for complex 2 [$(L_2)_2Cu^{II}$)].

Atoms	Bond Length (Å)	Atoms	Bond Angles (Å)
C(24)-C(39)	1.5011	Cl(37)-Cu(35)-Cl(36)	153.0356
C(7)-C(38)	1.4941	Cl(37)-Cu(35)-N(26)	86.7554
Cu(35)-Cl(37)	2.192	Cl(37)-Cu(35)-N(9)	87.8093
Cu(35)-Cl(36)	2.2093	Cl(37)-Cu(35)-N(21)	77.7928
Cu(35)-N(26)	1.4994	Cl(37)-Cu(35)-N(4)	107.7269
N(9)-Cu(35)	1.5554	Cl(36)-Cu(35)-N(26)	84.5678
Cu(35)-N(21)	1.4868	Cl(36)-Cu(35)-N(9)	117.1527
N(4)-Cu(35)	1.4893	Cl(36)-Cu(35)-N(21)	79.7548
C(19)-C(34)	1.5178	Cl(36)-Cu(35)-N(4)	86.9959
C(28)-C(33)	1.541	N(26)-Cu(35)-N(9)	87.3259
C(30)-C(32)	1.4839	N(26)-Cu(35)-N(21)	104.4614
C(23)-C(31)	1.4723	N(26)-Cu(35)-N(4)	161.4844
C(30)-C(25)	1.375	N(9)-Cu(35)-N(21)	160.6582
C(29)-C(30)	1.3708	N(9)-Cu(35)-N(4)	81.9097
C(28)-C(29)	1.3625	N(21)-Cu(35)-N(4)	90.1646
C(27)-C(28)	1.3555	C(32)-C(30)-C(25)	123.4304
N(26)-C(27)	1.2995	C(32)-C(30)-C(29)	118.6718
C(25)-N(26)	1.2757	C(25)-C(30)-C(29)	116.8379
C(24)-C(25)	1.4866	C(30)-C(29)-C(28)	116.1897
C(22)-C(24)	1.4765	C(33)-C(28)-C(29)	120.3641
C(23)-C(18)	1.3038	C(33)-C(28)-C(27)	124.9223
C(22)-C(23)	1.3486	C(29)-C(28)-C(27)	114.6384
N(21)-C(22)	1.2836	C(28)-C(27)-N(26)	124.7664
C(20)-N(21)	1.2876	Cu(35)-N(26)-C(27)	120.7064
C(19)-C(20)	1.3334	Cu(35)-N(26)-C(25)	128.8875
C(18)-C(19)	1.3441	C(27)-N(26)-C(25)	105.9906
C(2)-C(17)	1.5151	C(30)-C(25)-N(26)	120.5059
C(11)-C(16)	1.4444	C(30)-C(25)-C(24)	119.0134

Atoms	Bond Length (Å)	Atoms	Bond Angles (Å)
C(13)-C(15)	1.5213	N(26)-C(25)-C(24)	120.4788
C(6)-C(14)	1.5452	C(39)-C(24)-C(25)	101.6868
C(13)-C(8)	1.331	C(39)-C(24)-C(22)	117.1061
C(12)-C(13)	1.3291	C(25)-C(24)-C(22)	109.6494
C(11)-C(12)	1.3115	C(31)-C(23)-C(18)	108.5536
C(10)-C(11)	1.3335	C(31)-C(23)-C(22)	129.1917
N(9)-C(10)	1.3105	C(18)-C(23)-C(22)	121.3332
C(8)-N(9)	1.3215	C(24)-C(22)-C(23)	112.7108
C(7)-C(8)	1.5278	C(24)-C(22)-N(21)	124.0876
C(5)-C(7)	1.4967	C(23)-C(22)-N(21)	123.1962
C(6)-C(1)	1.4011	Cu(35)-N(21)-C(22)	126.8557
C(5)-C(6)	1.3411	Cu(35)-N(21)-C(20)	126.7866
N(4)-C(5)	1.2867	C(22)-N(21)-C(20)	104.0353
C(3)-N(4)	1.2756	N(21)-C(20)-C(19)	131.5285

Table S3. Calculated bond lengths and bond angles for complex 3 [(L1)2ZnII)].

Atoms	Bond Length (Å)	Atoms	Bond Length (Å)
Zn(35)-Cl(37)	2.269	Cl(37)-Zn(35)-N(26)	85.7276
Zn(35)-Cl(36)	2.2649	Cl(37)-Zn(35)-N(9)	89.9731
Zn(35)-N(26)	1.9879	Cl(37)-Zn(35)-N(21)	102.2592
N(9)-Zn(35)	1.9521	Cl(37)-Zn(35)-N(4)	159.2458
Zn(35)-N(21)	1.9254	Cl(36)-Zn(35)-N(26)	107.5712
N(4)-Zn(35)	1.9302	Cl(36)-Zn(35)-N(9)	83.8696
C(19)-C(34)	1.6044	Cl(36)-Zn(35)-N(21)	166.5796
C(28)-C(33)	1.5919	Cl(36)-Zn(35)-N(4)	81.3891
C(30)-C(32)	1.4925	N(26)-Zn(35)-N(9)	166.7972
C(23)-C(31)	1.5142	N(26)-Zn(35)-N(21)	59.7416
C(30)-C(25)	1.5554	N(26)-Zn(35)-N(4)	108.4661
C(29)-C(30)	1.5058	N(9)-Zn(35)-N(21)	109.2739
C(28)-C(29)	1.4289	N(9)-Zn(35)-N(4)	79.2426
C(27)-C(28)	1.4532	N(21)-Zn(35)-N(4)	98.0473
N(26)-C(27)	1.4343	C(32)-C(30)-C(25)	126.4791
C(25)-N(26)	1.7487	C(32)-C(30)-C(29)	117.2913
C(24)-C(25)	1.5345	C(25)-C(30)-C(29)	116.1028
C(22)-C(24)	1.4859	C(30)-C(29)-C(28)	123.2066
C(23)-C(18)	1.5042	C(33)-C(28)-C(29)	116.5832
C(22)-C(23)	1.4757	C(33)-C(28)-C(27)	117.8938
N(21)-C(22)	1.4031	C(29)-C(28)-C(27)	125.4919
C(20)-N(21)	1.3449	C(28)-C(27)-N(26)	121.5396
C(19)-C(20)	1.4845	Zn(35)-N(26)-C(27)	116.2009
C(18)-C(19)	1.8099	Zn(35)-N(26)-C(25)	121.4353
C(2)-C(17)	1.532	C(27)-N(26)-C(25)	115.9884
C(11)-C(16)	1.5511	C(30)-C(25)-N(26)	117.5975
C(13)-C(15)	1.5133	C(30)-C(25)-C(24)	117.5135
C(6)-C(14)	1.5137	N(26)-C(25)-C(24)	124.287
C(13)-C(8)	1.3619	C(25)-C(24)-C(22)	68.6123
C(12)-C(13)	1.3592	C(31)-C(23)-C(18)	122.2079
C(11)-C(12)	1.3333	C(31)-C(23)-C(22)	119.3633
C(10)-C(11)	1.3717	C(18)-C(23)-C(22)	113.9963
N(9)-C(10)	1.2605	C(24)-C(22)-C(23)	94.8046
C(8)-N(9)	1.258	C(24)-C(22)-N(21)	91.9129
C(7)-C(8)	1.5406	C(23)-C(22)-N(21)	126.812
C(5)-C(7)	1.4836	Zn(35)-N(21)-C(22)	98.6906
C(6)-C(1)	1.3242	Zn(35)-N(21)-C(20)	97.6709
C(5)-C(6)	1.3784	C(22)-N(21)-C(20)	122.8012
N(4)-C(5)	1.2906	N(21)-C(20)-C(19)	119.9407
C(3)-N(4)	1.2819	C(34)-C(19)-C(20)	104.1586
C(2)-C(3)	1.342	C(34)-C(19)-C(18)	139.8792

Table S4. Calculated bond lengths and bond angles for complex 4 [$(L_2)_2Zn^{II}$)].

Atoms	Bond Length (Å)	Atoms	Bond Length (Å)	Atoms	Bond Length (Å)
C(24)-C(39)	1.5532	Cl(37)-Zn(35)-Cl(36)	82.0567	C(7)-C(5)-N(4)	120.1775
C(7)-C(38)	1.5326	Cl(37)-Zn(35)-N(26)	84.2751	C(6)-C(5)-N(4)	118.842
Zn(35)-Cl(37)	2.2803	Cl(37)-Zn(35)-N(9)	86.0916	Zn(35)-N(4)-C(5)	121.5008
Zn(35)-Cl(36)	2.2342	Cl(37)-Zn(35)-N(21)	112.4484	Zn(35)-N(4)-C(3)	113.5931
Zn(35)-N(26)	1.9974	Cl(37)-Zn(35)-N(4)	159.5974	C(5)-N(4)-C(3)	117.7538
N(9)-Zn(35)	1.9295	Cl(36)-Zn(35)-N(26)	103.8557	N(4)-C(3)-C(2)	127.8502
Zn(35)-N(21)	1.9348	Cl(36)-Zn(35)-N(9)	85.3136	C(17)-C(2)-C(3)	122.7672
N(4)-Zn(35)	1.9478	Cl(36)-Zn(35)-N(21)	151.3749	C(17)-C(2)-C(1)	120.6978
C(19)-C(34)	1.611	Cl(36)-Zn(35)-N(4)	91.3758	C(3)-C(2)-C(1)	116.3747
C(28)-C(33)	1.5571	N(26)-Zn(35)-N(9)	165.615	C(6)-C(1)-C(2)	116.2958
C(30)-C(32)	1.4927	N(26)-Zn(35)-N(21)	55.9494	C(7)-C(5)-N(4)	120.1775
C(23)-C(31)	1.5193	N(26)-Zn(35)-N(4)	116.0991	C(6)-C(5)-N(4)	118.842

Atoms	Bond Length (Å)	Atoms	Bond Length (Å)	Atoms	Bond Length (Å)
C(30)-C(25)	1.556	N(9)-Zn(35)-N(21)	119.0257	Zn(35)-N(4)-C(5)	121.5008
C(29)-C(30)	1.4598	N(9)-Zn(35)-N(4)	74.0877	Zn(35)-N(4)-C(3)	113.5931
C(28)-C(29)	1.3961	N(21)-Zn(35)-N(4)	82.169	C(5)-N(4)-C(3)	117.7538
C(27)-C(28)	1.4537	C(32)-C(30)-C(25)	124.9559	N(4)-C(3)-C(2)	127.8502
N(26)-C(27)	1.3959	C(32)-C(30)-C(29)	115.6976	C(17)-C(2)-C(3)	122.7672
C(25)-N(26)	1.7228	C(25)-C(30)-C(29)	119.3428	C(17)-C(2)-C(1)	120.6978
C(24)-C(25)	1.5681	C(30)-C(29)-C(28)	120.2622		
C(22)-C(24)	1.4265	C(33)-C(28)-C(29)	113.5367		
C(23)-C(18)	1.4629	C(33)-C(28)-C(27)	120.4952		
C(22)-C(23)	1.4795	C(29)-C(28)-C(27)	125.4173		
N(21)-C(22)	1.3771	C(28)-C(27)-N(26)	124.1029		
C(20)-N(21)	1.3763	Zn(35)-N(26)-C(27)	103.4777		
C(19)-C(20)	1.8839	Zn(35)-N(26)-C(25)	117.8867		
C(18)-C(19)	1.4797	C(27)-N(26)-C(25)	113.6982		
C(2)-C(17)	1.5122	C(30)-C(25)-N(26)	116.2527		
C(11)-C(16)	1.516	C(30)-C(25)-C(24)	111.2925		
C(13)-C(15)	1.5087	N(26)-C(25)-C(24)	125.2356		
C(6)-C(14)	1.5105	C(39)-C(24)-C(25)	111.596		
C(13)-C(8)	1.3391	C(39)-C(24)-C(22)	121.3892		
C(12)-C(13)	1.3332	C(25)-C(24)-C(22)	76.8332		
C(11)-C(12)	1.3336	C(31)-C(23)-C(18)	115.8536		
C(10)-C(11)	1.3153	C(31)-C(23)-C(22)	119.5661		
N(9)-C(10)	1.2889	C(18)-C(23)-C(22)	123.9732		
C(8)-N(9)	1.2881	C(24)-C(22)-C(23)	97.0672		
C(7)-C(8)	1.5179	C(24)-C(22)-N(21)	87.1718		
C(5)-C(7)	1.52	C(23)-C(22)-N(21)	120.5302		
C(6)-C(1)	1.3514	Zn(35)-N(21)-C(22)	99.4721		
C(5)-C(6)	1.3581	Zn(35)-N(21)-C(20)	96.6989		
N(4)-C(5)	1.2489	C(22)-N(21)-C(20)	122.661		
C(3)-N(4)	1.2437	N(21)-C(20)-C(19)	115.5581		
C(2)-C(3)	1.3498	C(34)-C(19)-C(20)	140.7457		

Table S5. Calculated atomic charges for the copper (II) complexes.

$[(L_1)_2Cu^{II}]$		Atomic	Charges	$[(L_2)_2Cu^{II}]$		Atomic	Charges
Number	Atom	LOEWDIN	MULLIKEN	Number	Atom	LOEWDIN	MULLIKEN
0	C	0.06656	0.26641	0	C	-0.123747	0.114082
1	N	-0.111968	-0.57661	1	N	0.206564	0.342053
2	N	-0.073949	-0.528931	2	N	0.105165	0.177428
3	C	-0.024903	0.152229	3	C	-0.237952	0.138524
4	C	0.097378	-0.083498	4	C	-0.022796	-0.024197
5	C	0.024067	-0.19049	5	C	-0.096729	0.064172
6	C	0.05647	-0.071276	6	C	-0.146483	-0.06161
7	C	0.156242	0.162011	7	C	-0.199086	0.150787
8	C	-0.065199	-0.140245	8	C	-0.089622	-0.1399
9	C	0.090096	0.188531	9	C	-0.235694	0.085726
10	C	-0.065494	-0.104275	10	C	-0.106819	-0.165471
11	C	-0.041254	0.014805	11	C	-0.287523	-0.366794
12	C	-0.032741	0.037344	12	C	-0.254521	-0.529801
13	C	-0.024526	0.078746	13	C	-0.244586	-0.390814
14	C	-0.015039	0.098096	14	C	-0.24313	-0.394826
15	C	0.08065	0.233607	15	C	-0.075849	0.207632
16	N	-0.230899	-0.735462	16	N	0.107349	0.256319
17	N	-0.072142	-0.511559	17	N	0.11064	0.161191
18	C	-0.052032	0.202028	18	C	-0.223786	0.196524
19	C	0.136581	0.046366	19	C	-0.017231	-0.053333
20	C	0.07045	-0.127745	20	C	-0.099506	-0.064967
21	C	0.070707	-0.05507	21	C	-0.090454	0.016979
22	C	0.128391	0.063402	22	C	-0.193622	0.242559
23	C	-0.096614	-0.171133	23	C	-0.071967	-0.198286
24	C	0.130654	0.204266	24	C	-0.20287	-0.041858
25	C	-0.092755	-0.103608	25	C	-0.099418	-0.119115
26	C	-0.032656	0.057016	26	C	-0.272221	-0.362053
27	C	-0.028571	0.025821	27	C	-0.289431	-0.356499
28	C	-0.021303	0.066716	28	C	-0.241183	-0.377323
29	C	-0.017397	0.08479	29	C	-0.231157	-0.426101
30	C	0.156556	0.887488	30	C	-0.350372	-0.92555
31	C	-0.162565	-0.389819	31	C	0.116806	-0.431927
32	C	-0.379588	-0.599645	32	C	0.288028	-0.27341
33	H	0.057266	0.128178	33	C	-0.231981	-0.415144
34	H	0.0426	0.089799	34	C	-0.226589	-0.45162
35	H	0.044397	0.06112	35	H	0.207041	0.148559
36	H	0.040936	0.058477	36	H	0.161407	0.130661
37	H	0.026222	0.08798	37	H	0.166401	0.140011

$[(L_1)_2Cu^{II}]$		Atomic	Charges	$[(L_2)_2Cu^{II}]$		Atomic	Charges
38	H	0.035927	0.06352	38	H	0.121031	0.176619
39	H	0.044582	0.073927	39	H	0.146088	0.153212
40	H	0.053231	0.094826	40	H	0.140951	0.130581
41	H	0.03363	0.062525	41	H	0.143528	0.167314
42	H	0.034818	0.090156	42	H	0.137115	0.146112
43	H	0.033105	0.059352	43	H	0.132127	0.172155
44	H	0.040617	0.072088	44	H	0.141161	0.14462
45	H	0.04323	0.071864	45	H	0.142677	0.147788
46	H	0.046611	0.084704	46	H	0.13999	0.140997
47	H	0.047726	0.079671	47	H	0.127836	0.129865
48	H	0.036456	0.066063	48	H	0.136862	0.146262
49	H	0.075802	0.151671	49	H	0.138912	0.138737
50	H	0.057903	0.095838	50	H	0.201111	0.11368
51	H	0.039832	0.053305	51	H	0.166987	0.146519
52	H	0.037045	0.052023	52	H	0.171403	0.15299
53	H	0.032708	0.059362	53	H	0.138882	0.170789
54	H	0.044368	0.088579	54	H	0.133508	0.12583
55	H	0.037866	0.060042	55	H	0.147204	0.164115
56	H	0.047447	0.088105	56	H	0.144599	0.169591
57	H	0.029574	0.079523	57	H	0.132593	0.125729
58	H	0.04697	0.082152	58	H	0.125101	0.158081
59	H	0.043061	0.077519	59	H	0.139752	0.138749
60	H	0.043165	0.075939	60	H	0.142594	0.160986
61	H	0.046795	0.077337	61	H	0.144502	0.144213
62	H	0.042319	0.076697	62	H	0.138728	0.152933
63	H	0.044558	0.073031	63	H	0.142383	0.155052
64	H	0.046026	0.08432	64	H	0.144879	0.15344

Table S6. Calculated atomic charges for the zinc (II) complexes.

$[(L_1)_2Zn^{II}]$		Atomic	Charges	$[(L2)_2Zn^{II}]$		Atomic	Charges
Number	Atom	LOEWDIN	MULLIKEN	Number	Atom	LOEWDIN	MULLIKEN
0	C	-0.13389	0.059014	0	C	0.056854	0.230384
1	N	0.236658	0.077325	1	N	-0.29592	-0.75827
2	N	0.283684	0.138386	2	N	0.184077	-0.1933
3	C	-0.23899	0.150813	3	C	-0.08081	0.053721
4	C	0.07668	-0.13179	4	C	0.280265	-0.0204
5	C	-0.02911	0.096331	5	C	0.069669	-0.19425
6	C	-0.03523	0.091239	6	C	0.272675	0.080186
7	C	-0.16072	0.230236	7	C	0.121901	-0.00106
8	C	0.007457	-0.15005	8	C	-0.01958	-0.07132
9	C	-0.19878	0.199476	9	C	0.139303	0.155759
10	C	-0.02514	-0.09657	10	C	-0.05974	-0.08125
11	C	-0.21863	-0.48008	11	C	-0.04128	-0.00528
12	C	-0.20635	-0.43959	12	C	-0.01738	0.082916
13	C	-0.20587	-0.37387	13	C	-0.02027	0.042633
14	C	-0.18866	-0.35542	14	C	0.000961	0.036146
15	Z	-0.64052	-0.34013	15	Z	0.478159	0.936406
16	C	0.295671	-0.14413	16	C	-0.10634	-0.30212
17	C	0.247524	-0.2211	17	C	-0.37863	-0.53371
18	C	-0.17126	-0.10522	18	C	0.1897	-0.00992
19	N	0.270787	-0.18971	19	N	-0.18588	-0.53844
20	N	0.284814	-0.05478	20	N	0.248834	-0.07286
21	C	-0.11634	0.262012	21	C	-0.14917	-0.02214
22	C	-0.0635	-0.32228	22	C	0.197653	-0.19005
23	C	0.146662	0.075122	23	C	0.062257	-0.15461
24	C	0.037443	-0.02247	24	C	-0.03824	-0.26197
25	C	-0.03465	0.150074	25	C	0.216852	0.397512
26	C	0.199543	0.067997	26	C	0.011249	-0.21416
27	C	-0.39764	0.365	27	C	0.140372	0.170821
28	C	-0.15567	-0.33151	28	C	-0.0382	-0.07804
29	C	-0.37581	-0.41033	29	C	-0.01598	0.023408
30	C	-0.19573	-0.22211	30	C	0.005488	0.019738
31	C	-0.19177	-0.22205	31	C	-0.01133	0.039895
32	C	-0.15953	-0.25585	32	C	0.02698	0.162435
33	H	0.222427	0.226468	33	C	-0.00866	-0.03304
34	H	0.195117	0.232617	34	C	0.040635	0.084539
35	H	0.187468	0.201149	35	H	0.077548	0.174448
36	H	0.189917	0.213106	36	H	0.091415	0.160108
37	H	0.134447	0.165197	37	H	0.073318	0.129821
38	H	0.165666	0.207596	38	H	0.029046	0.094093
39	H	0.169044	0.207984	39	H	0.086873	0.158454
40	H	0.153669	0.169023	40	H	0.068576	0.126493
41	H	0.152591	0.188848	41	H	0.025411	0.035798
42	H	0.166459	0.204043	42	H	0.071735	0.133664

$[(L_1)_2Zn^{II}]$		Atomic	Charges	$[(L2)_2Zn^{II}]$		Atomic	Charges
43	H	0.164815	0.185032	43	H	0.091927	0.179292
44	H	0.171035	0.19569	44	H	0.055009	0.104837
45	H	0.160556	0.18885	45	H	0.071015	0.131087
46	H	0.168306	0.190239	46	H	0.054301	0.105391
47	H	0.159923	0.181957	47	H	0.105129	0.188127
48	H	0.168959	0.190881	48	H	0.078855	0.144717
49	H	0.296555	0.261325	49	H	0.087522	0.161684
50	H	0.19167	0.241164	50	H	0.111323	0.227843
51	H	0.239882	0.315389	51	H	0.100225	0.205708
52	H	0.193833	0.192929	52	H	0.079005	0.139945
53	H	0.246153	0.251583	53	H	0.095005	0.16785
54	H	0.269298	0.254949	54	H	0.022812	0.066048
55	H	0.220205	0.221301	55	H	0.069859	0.130118
56	H	0.170018	0.203738	56	H	0.078564	0.148485
57	H	0.174987	0.198896	57	H	0.08866	0.167739
58	H	0.181756	0.233421	58	H	0.109834	0.182747
59	H	0.199345	0.24351	59	H	0.050816	0.101405
60	H	0.197846	0.232535	60	H	0.071288	0.132476
61	H	0.190531	0.222231	61	H	0.077486	0.144338
62	H	0.190389	0.244185	62	H	0.069981	0.160107
63	H	0.182854	0.225663	63	H	0.057923	0.122213
64	H	0.181157	0.214515	64	H	0.045459	0.116009
				65	H	0.068499	0.135739
				66	H	0.080455	0.156817
				67	H	0.090225	0.176027
				68	H	0.099214	0.168014
				69	H	0.095819	0.180856
				70	H	0.093409	0.161164